Spectroscopy of chromium centers in $LiScGeO_4$ and $LiInGeO_4$ single crystals

M. Yu. Sharonov, A. B. Bykov, P. Rojas, V. Petricevic, and R. R. Alfano
Institute for Ultrafast Spectroscopy and Lasers, Department of Physics, The City College and Graduate School of the City University of New York, New York, New York 10031, USA
(Received 1 April 2005; published 14 September 2005)

The detailed spectroscopy of $Cr:LiScGeO_4$ and $Cr:LiInGeO_4$ is presented. Low temperature absorption, emission, and excitation spectroscopies reveal two types of optical centers: trivalent chromium in the distorted octahedral sites and tetravalent chromium in the tetrahedral sites. Energies of the transitions calculated from the exact atom positions using the angular overlap model are in a satisfactory agreement with the experimental data and describe the unusually low energy position of the Cr^{3+} metastable level. The spin-forbidden ^2E and $^2T_1$ transitions of Cr^{3+} appear as a Fano antiresonance in the absorption and excitation spectra. The temperature quenching of Cr^{3+} fluorescence is described in terms of the Struck and Fonger model. Cr^{3+} ions in highly distorted octahedral positions are active centers responsible for recently discovered Cr^{3+} laser action in the near-infrared range in these crystals.

DOI: 10.1103/PhysRevB.72.115111 PACS number(s): 78.20.−e, 71.70.Ch, 42.70.−a

I. INTRODUCTION

Since Cr^{3+} doped tunable lasers were discovered in the early 1980s they have attracted great interest because of a wide range of possible applications. The range of tunability of known Cr^{3+} doped materials is from 700 nm [for alexandrite, $BeAl_2O_6$ (Ref. 1)] to 1107 nm [for $La_3Ga_5SiO_{14}$ (Ref. 2)]. The range of tunable laser operation was extended to the near infrared range with the discovery of tunable laser operation in forsterite[3] and YAG.[4] The assignment of electronic transitions to Cr^{4+} ions in these crystals has generated growing interest in Cr^{4+} based laser materials. Tetrahedral surrounding of Cr^{4+} ions produces lower crystal field than octahedral surrounding of Cr^{3+} ions, therefore the range of operation of Cr^{4+}-doped materials is typically shifted toward lower energies than the range of operation of Cr^{3+} doped materials. Attempts to achieve near-infrared laser action from Cr^{3+} ions in octahedral positions were unsuccessful because of strong nonradiative quenching of the fluorescence.[5,6] These experimental results lead to the trend to consider chromium in the tetravalent state as the only available valence state for laser operation in the near infrared region.

In our recent work, we have demonstrated laser action in two new chromium doped crystals $LiScGeO_4$ and $LiInGeO_4$ in the range 1150–1480 nm for $LiInGeO_4$ and 1220–1380 for $LiScGeO_4$, respectively.[7] These crystals exhibit unusual fluorescence in the near-infrared range. Preliminary spectroscopic study revealed two types of optical centers, assigned to octahedrally coordinated Cr^{3+} and tetrahedrally coordinated Cr^{4+}. Based on this study we have assigned laser action to Cr^{3+} centers rather than Cr^{4+} centers (previously, we reported chromium-doped $LiScGeO_4$ as a laser material,[8] but emission was incorrectly assigned to the tetrahedral Cr^{4+} centers). To our knowledge this was the first demonstration of laser operation of Cr^{3+} centers in the near infrared (NIR) region.[7,8]

In this paper, we present spectroscopy of both Cr^{3+} and Cr^{4+} centers in detail. Low temperature absorption, emission, and excitation spectra are analyzed in terms of the angular overlap model (AOM) and Fano-antiresonance effect; and the nonradiative quenching of fluorescence is analyzed on the basis of the Struck and Fonger model. This detailed study clarifies electronic structure and energy transfer in these promising and extremely wideband NIR materials.

II. EXPERIMENT

A. Crystal growth and spectroscopic measurements

Crystals were grown by the conventional flux (solution) method by use of a Bi_2O_3-based solvent. Chromium content in the flux was ~2 wt % of Cr_2O_3. Bulk crystals of size up to 1 cm × 1 cm × 2 cm in size grew on the bottom of the crucible. Although the crystals were severely solvent entrapped, relatively large $LiInGeO_4$ and $LiScGeO_4$ transparent plates suitable for spectroscopic and laser experiments were prepared. Spontaneous crystallization is characterized by anisotropic incorporation of an impurity in the crystals; it usually appears as stripes of different colors that are clearly visible under an optical microscope. Impurity incorporation in the crystal during high-temperature growth from solution (spontaneous or crystallization on seeds) always varies with growth temperature and it is very sensitive to any changes in growth kinetics (growth rate, growth direction, and others). In our case, it led to variable chromium concentration in the crystals taken from different parts of the crucible (bottom, walls, or melt surface), as well as different parts of the crystal (core and surface area) which are characterized by the inhomogeneous chromium distribution. As a result, the total amount and relative contents of Cr^{3+} and Cr^{4+} centers that depend on growth parameters varies from crystal to crystal. Details of crystal growth are described in Refs. 9 and 10 for $Cr:LiScGeO_4$ and $Cr:LiInGeO_4$, respectively.

Absorption spectra were measured on a Cary 500 double beam spectrophotometer. Spontaneous emission spectra were measured on excitation with an Ar laser (488, 514.5 nm lines) and a 670 nm laser diode. Excitation spectra were recorded on excitation with a 1000 W tungsten lamp or Xe arc lamp dispersed through the McPherson 0.3-m monochromator. Decay curves were measured on excitation with a

Ti:sapphire laser (at 800 nm) pumped with Q-switched pulses of a second harmonic YAG:Nd laser. Decay traces were recorded on a Tektronix TDS 684a oscilloscope and where transferred to a PC. To improve the signal-to-noise ratio 300–1000 traces were averaged for each measurement. For low temperature measurements a helium close-cycle Janis Research cryostat was used with the range of 10–360 K. AOM calculations were performed with the computer program developed by us[11] and with the AOMX program.[12]

B. Crystal structure

$LiScGeO_4$ and $LiInGeO_4$ belong to the olivine group of crystals, similar to well-known Cr^{4+}-doped laser crystals $Cr^{4+}:Mg_2SiO_4$ (forsterite),[3] $Cr^{4+}:Ca_2GeO_4$ (cunyite),[13] and Cr^{3+}-doped $BeAl_2O_4$ (alexandrite). In this paper *Pnma* notation of the crystal space group is used. This group indicates a rectangular ($\alpha=\beta=\gamma=\pi/2$) primitive cell with unequal lattice constant, the unit cell has the following dimensions: $a=1.0673$ nm, $b=0.5993$ nm, and $c=0.4967$ nm for $LiScGeO_4$ crystals[14] and $a=1.0754$, $b=0.6088$, and $c=0.5007$ for $LiInGeO_4$ crystals.[15] There are two major types of sites in the olivine lattice: distorted octahedrons and distorted tetrahedrons. The chromium in Cr-doped Mg_2SiO_4 can occupy both octahedral (Cr^{3+}) (two different 4*a* and 4*c* sites) and tetrahedral (Cr^{4+}) positions; the relative content of Cr^{3+} and Cr^{4+} depends on growing conditions.[16] In forsterite, Cr^{4+} in tetrahedral positions is responsible for laser action, whereas Cr^{3+} in octahedral coordination was not found to be a laser ion because of Cr^{3+} emission overlapped with the absorption of divalent and tetravalent centers. The formation of Cr^{3+} centers in Ca_2GeO_4 is avoided by replacing the Mg^{2+} ion with a much larger Ca^{2+} ion, thus in Ca_2GeO_4 only Cr^{4+} centers are possible. In $LiScGeO_4$ and $LiInGeO_4$ crystals both octahedral and tetrahedral centers can be occupied by chromium in trivalent (octahedral centers) and tetravalent (tetrahedral centers) states. Cr^{3+} centers in $Cr:LiScGeO_4$ were detected by electron paramagnetic resonance (EPR) in octahedral 4*c* sites.[17]

III. RESULTS

A. Absorption

Figure 1 shows polarized absorption spectra of $Cr:LiScGeO_4$ crystal, at 20 K. $E\|a$ polarization is shown by a dotted curve, $E\|b$ polarization is shown by a dashed curve, and $E\|c$ polarization is shown by a thin solid curve. The tops of the bands for $E\|a$ and $E\|c$ are affected by saturation of the spectrometer (we used samples of ~2 mm thickness to get better resolution of the weak bands), the "corrected" profiles are shown by a dash-dot-dash line. The bands are indicated with roman numerals. Spectra show several absorption bands typical for Cr^{4+} in tetrahedral environment. Strongly polarized peaks of the absorption bands at ~12 500 nm (IV), ~15 000 nm (III), and ~17 000 nm (II) are attributed to the low-symmetry components of the $^3T_1$ tetrahedral state of the Cr^{4+} ion. Weak absorption bands at 8000–10 000 cm^{-1} (V) are attributed to the components of $^3T_2$ state, this area is shown in the insert in Fig 1; the zero-phonon line is indicated as 0-0. Similar to forsterite (Mg_2SiO_4) and cunyite (Ca_2GeO_4) crystals, the lowest $^3T_2$ band shows a sharp zero-phonon line and its phonon repetitions.[18] strong band at ~21 000 cm^{-1} (I) was not observed in Cr^{4+} doped forsterite and cunyite, but this band exists in Cr^{3+} forsterite and is assigned to the $^4T_1$ band of octahedrally coordinated Cr^{3+}. Similar absorption spectrum for $Cr:LiInGeO_4$ is shown in Fig. 2. Absorption at 6000–10 000 cm^{-1}($E\|a$) is much weaker for $Cr:LiInGeO_4$ than for $Cr:LiScGeO_4$ (see bump indicated as V in Figs. 1 and 2 for $E\|a$). For both $Cr:LiScGeO_4$ and $Cr:LiInGeO_4$ sharp lines are clearly seen at ~14 600 cm^{-1}. These lines were not observed in other olivines doped with tetravalent chromium. The lines are discussed below.

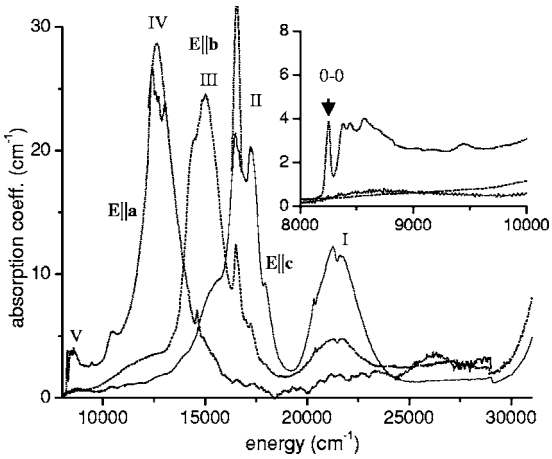

FIG. 1. Polarized absorption spectra of $Cr:LiScGeO_4$ crystal at 20 K. $E\|a$ polarization is shown by a dotted curve, $E\|b$ polarization is shown by a dashed curve, and $E\|c$ polarization is shown by a solid curve. The tops of the bands for $E\|a$ and $E\|c$ are affected by saturation of the spectrometer, the "corrected" profiles are shown by a dash-dot-dash curve. The inset shows low-energy region at higher resolution, zero-phonon line is indicated by 0-0.

Since there are both Cr^{3+} and Cr^{4+} centers in the lattice, absorption bands are not "pure" Cr^{4+} or Cr^{3+} bands. Bands in

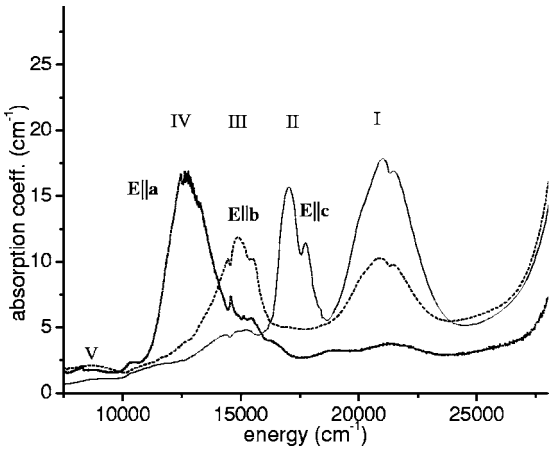

FIG. 2. Polarized absorption spectra of $Cr:LiInGeO_4$ at 20 K. $E\|a$ polarization is shown by a dotted curve, $E\|b$ polarization is shown by a dashed curve, and $E\|c$ polarization is shown by a solid curve.

TABLE I. The ratio of the intensity of selected transitions to the intensity of the transition at 17 000 cm^{-1} for $E\|c$ at room temperature (the ratio for the transition II is always 1, because this transition is used for normalization).

	The ratio of the intensity of the specified absorption band to the intensity of the absorption band at ~17 000 cm^{-1}, $E\|c$					
Sample	I ~21 000 cm^{-1} $E\|c$	II ~17 000 cm^{-1} $E\|c$	III ~15 000 cm^{-1} $E\|b$	IV ~12 500 cm^{-1} $E\|a$	V ~8500 cm^{-1} $E\|a$	Laser action
			$LiScGeO_4$			
A	0.27	1	0.52	0.47	0.038	No
B	0.73	1	0.62	0.67	0.033	Yes
			$LiInGeO_4$			
A	1.09	1	0.65	1.05	~0.011	No
B	1.61	1	0.76	1.47	~0.008	Yes

the near-infrared located at 7000–10 000 cm^{-1} belong primarily to Cr^{4+} $^3T_2$ transitions (the "vibronic progression" shape and location of these bands are very similar to those in other Cr^{4+} doped olivine crystals). The band at 21 000 cm^{-1} belongs primarily to the Cr^{3+} $^4T_1$ transition (because a similar strong band exists in Cr^{3+} doped forsterite). Bands in the range 10 000–20 000 cm^{-1} can be a composition of both Cr^{3+} and Cr^{4+} bands, because both of these ions have strong absorption in this range. The ratios of intensities of the above-mentioned bands depend on growing conditions and reflect the relative content of Cr^{3+} and Cr^{4+} ions. Ratios of some selected transition to the intensity of the peak at 17 000 cm^{-1}($E\|c$) (one of the most typical Cr^{4+} lines assigned to the highest components of $^3T_1$ state) for several samples of the studied crystals at room temperature are listed in Table I. A and B indicate samples cut from different samples where the relative content of Cr^{3+} and Cr^{4+} ions is different (clearly distinguished by different coloring of the samples; even so content of Cr in the flux was the same in all crystal grow experiments. The valency of chromium was determined by growing conditions rather than by different flux composition). In Table I columns are marked by roman numerals for some selected electronic transitions: (I) denotes this ratio for the transition at ~21 000 cm^{-1} for $E\|c$; (II) is the ratio for the transition at ~17 000 cm^{-1} for $E\|c$ (this ratio is always equal to 1, because this transition is used for normalization); (III) is the ratio for the transition at 15 000 cm^{-1} for $E\|b$; (IV) is the ratio at ~12 500 cm^{-1} for $E\|a$; and (V) is the ratio at 8500 cm^{-1} for $E\|a$. The roman numeral notation of the bands corresponds to the notation used in Figs. 1 and 2.

As we discussed above, transition I is attributed mainly to the $^4T_1$ absorption of Cr^{3+}, transitions II and V are attributed mainly to Cr^{4+} transitions, transitions III and IV can be a sum of $Cr^{3+}(^4T_2)$ and $Cr^{4+}(^3T_1)$ transitions. In agreement with our suggestion on the assignment of Cr^{3+} and Cr^{4+} transitions, the most noticeable change is for the transition I. This ratio represents relative content of Cr^{3+} and Cr^{4+}: higher relative content of Cr^{3+} corresponds to the higher ratio of $^4T_1(Cr^{3+})$ to $^3T_1(Cr^{4+})$. Laser action was obtained only for the samples with relatively small content of Cr^{4+}, where there is no strong absorption of Cr^{3+} radiation by Cr^{4+} $^3T_2$ transitions.[7]

B. Emission

Fluorescence spectra of $Cr:LiScGeO_4$ and $Cr:LiInGeO_4$ crystals at room temperature (solid line) and 10 K (dotted line) are shown in Figs. 3(a) and 3(b), respectively. For reference, in Fig. 3(a) the low temperature absorption spectrum of $Cr:LiScGeO_4$ for $E\|a$ is also shown. In contrast to Cr^{4+} doped forsterite and cunyite, the fluorescence spectra are broadband and structureless even at low temperature. Weak structure at ~8000 cm^{-1} most probably is caused by $^3A_2$ - $^3T_1$ absorption of Cr^{4+}. Maxima of the fluorescence spectra are located at 9100 cm^{-1}(1100 nm) and 8670 cm^{-1}(1153 nm) for $LiScGeO_4$ and $LiInGeO_4$ crystals, respectively. Fluorescence begins well above the metastable level of Cr^{4+}, this fact excludes the $^3T_2$ state of Cr^{4+} as an origin of the fluorescence.

The spectra are the same on excitation with 488, 514.5, and 670 nm laser sources. Surprisingly, we did not find any fluorescence from the Cr^{4+} $^3T_2$ states neither at room nor at low temperature for any of our samples (even with high Cr^{4+} content); for these measurements we used a Nd:YAG laser to pump Cr^{4+} ions directly through the $^3T_2$ absorption band. Complete lack of the emission from Cr^{4+} centers in these crystals can be explained by strong nonradiative quenching. This is rather unusual for germanate and silicate olivines, but was observed in many other Cr^{4+} doped crystals.

Decay of the fluorescence measured on excitation by a pulsed Ti:sapphire laser at 800 nm is single exponential in the whole temperature range (10–360 K) and the lifetime of the decay stays the same within the range of the fluorescence (but depends on temperature as discussed later). The independence of the lifetime on the wavelength of fluorescence indicates that fluorescence originates from the single type of optical centers.

C. Excitation spectra

Polarized excitation spectra of $LiScGeO_4$ and $LiInGeO_4$ at 10 K are shown in Figs. 4 and 5, respectively (by a dotted

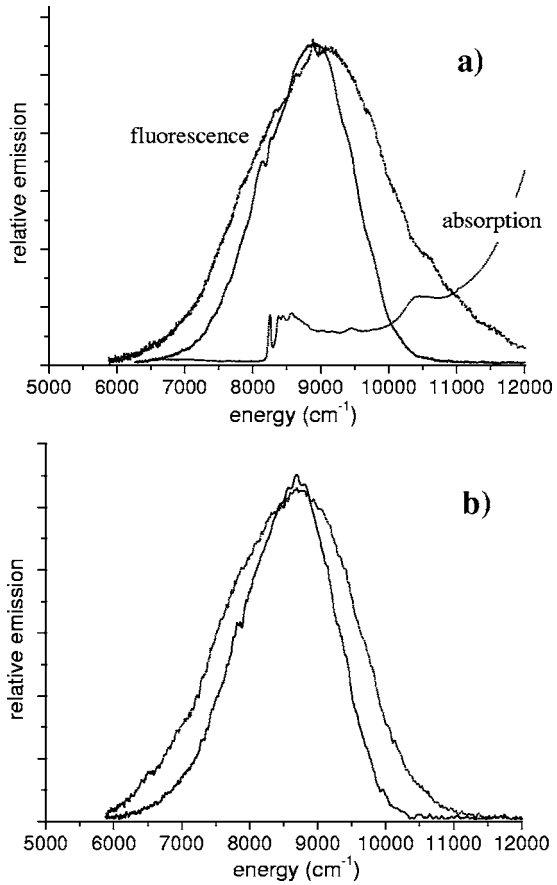

FIG. 3. (a) Emission spectrum of $Cr:LiScGeO_4$ at room temperature (dotted curve) and 20 K (solid curve), the reference absorption spectrum at 20 K for $E\|a$ is shown by a dashed curve; and (b) emission spectrum of $Cr:LiInGeO_4$ at room temperature (dotted curve) and 20 K (solid curve).

curve for $E\|a$, by a dashed curve for $E\|b$ and by a solid curve for $E\|c$). Emission was monitored at the maximum of the fluorescence band at $\sim$9000 cm^{-1}. There are two major bands in the spectra located at $\sim$14 000 and $\sim$21 000 cm^{-1}. Excitation spectra are very different from the absorption spectra where there are three typical for $^3T_1$ transition of Cr^{4+} strongly polarized bands at $\sim$12 500, $\sim$15 000, and $\sim$17 000 cm^{-1}. We assign two bands observed in the excitation spectra to $^4T_2(\sim 14\,000\ \text{cm}^{-1})$ and $^4T_1(\sim 21\,000\ \text{cm}^{-1})$ transitions of Cr^{3+} octahedral centers. This assignment is in agreement with an intensity analysis of the absorption spectra discussed above. Cr^{3+} octahedra are strongly distorted; and this distortion produces low-symmetry splitting of $^4T_2$ transitions into three components. Axes of the octahedral sites are not parallel to the crystal axes; there are always several projections of the octahedron axes to any certain axis of the crystal. This leads to the relatively weak dependence on polarization and to the complex structure of the bands at any polarization. The structure and orientation of Cr^{3+} octahedral sites is discussed below. At the high-energy side of the $^4A_2$-$^4T_2$ band there is a fine structure in the profile of the band clearly seen also in the low-temperature absorption spectra. The inset to Fig. 4 shows this fine structure together with the smooth background of the transition (shown by a

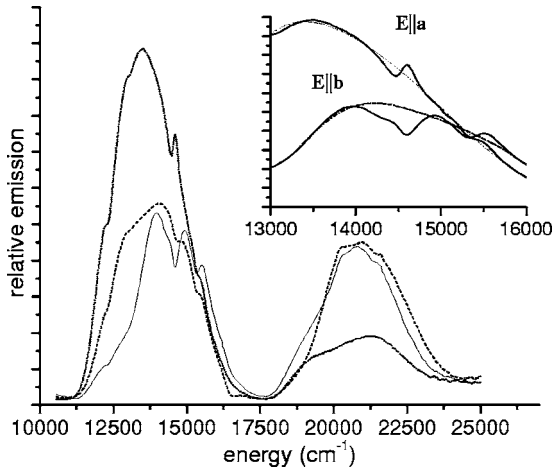

FIG. 4. Polarized excitation spectra of the emission (monitored at $\sim$9000 cm^{-1}) in $Cr:LiScGeO_4$ ($E\|a$ is shown by a dotted curve, $E\|b$ is shown by a dashed curve, and $E\|c$ is shown by a solid curve) at 20 K. The inset shows the region of sharp lines at higher resolution.

dotted line). The fine structure has "derivative-like" behavior and is very similar to the structure observed in some Cr^{3+} glasses and crystals.[19,20] This structure appears due to interaction of the sharp spin-forbidden $^4A_2$-^2E and $^4A_2$-$^2T_1$ transitions with the wideband vibronic $^4T_2$ state.

The structure shown in Figs. 4 and 5 can be described in terms of Fano theory (originally developed for gases[21] and later modified to solids by Struge *et al.*[22]). Fano antiresonance is described as an interference between sharp forbidden transition to an excited state and a broadband "continuum." A fraction of vibronic $^4T_2$ state interacts with the sharp transition (^2E, $^2T_1$). The spin-orbit interaction is responsible for the interference of states. The profile in the absorption spectrum is characterized by parameters of the interaction and has in general dispersionlike shape at the

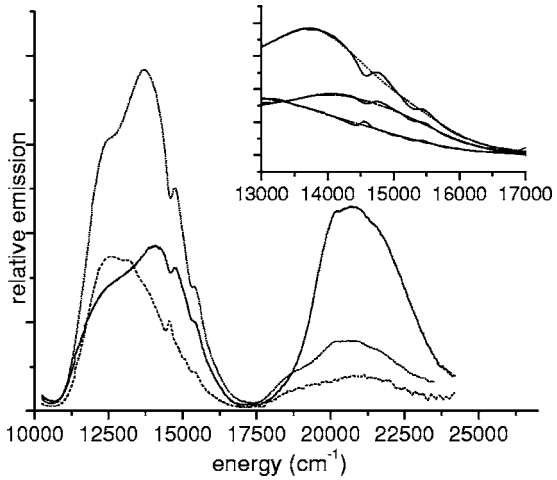

FIG. 5. Polarized excitation spectra of the emission (monitored at $\sim$9000 cm^{-1}) in $Cr:LiInGeO_4$ ($E\|a$ is shown by a dotted curve, $E\|b$ is shown by a dashed curve, and $E\|c$ is shown by a solid curve) at 20 K. The inset shows the region of sharp lines at higher resolution.

resonance frequency ω_r. The analysis of the profile and obtaining of the parameters of the theory is very sensitive to the correct subtraction of the background. In our case the situation becomes even more complicated, since we have a sum of low-symmetry spitted components of both sharp ^2E, $^2T_1$ and broadband $^4T_2$ transitions in all polarizations. All this makes fitting the shape unreasonable, and therefore parameters of theory cannot be determined. ω_r differs from the frequency of "pure" sharp ^2E or $^2T_1$ transitions (Lamb shift), uncertainty in the ω_r parameter and other parameters makes it impossible to find the position of "pure" ^2E and $^2T_1$ states with the accuracy more than ~ 100 cm^{-1}.

IV. DISCUSSION

A. Structure of chromium centers and energy level calculations

$LiScGeO_4$ and $LiInGeO_4$ belong to the olivine group of crystals. This group has an orthorhombic structure with the space group P_{nma} and contains four formula units per unit cell. There are two possible positions for chromium ions: (a) Ge tetrahedrons and (b) Sc or In (for $LiScGeO_4$ and $LiInGeO_4$, respectively) octahedrons. In the sites of (a) type, Ge is replaced by tetravalent chromium; in the (b) sites Sc or In is replaced by trivalent chromium. In contrast to forsterite, where there are two inequivalent octahedral positions for trivalent chromium (4a and 4c sites) and one for tetravalent chromium; in these crystals there is only one octahedral (4c) and one tetrahedral position for the chromium ions in the trivalent and the tetravalent states, respectively. Octahedral 4*a* sites are occupied by Li-ions and the Li-ions are not substitutable by Cr^{3+} ions (such substitution is difficult from a crystallochemical point of view; absence of such substitution was proven by EPR study[17] for $Cr:LiScGeO_4$). Atom positions and geometry of optical centers were derived from structural data published in Ref. 14 for $LiScGeO_4$ Ref. 15 for $LiInGeO_4$. Ligand field analysis was performed using the angular overlap model (AOM). One e_σ and one e_π parameter were used to describe Cr—O bonding. This assumption is better for tetrahedrons where Ge—O distances vary within 2.5% and is not as good for octahedrons, where Sc, In—O distances vary within 7%. The C/B parameter was fixed to the value for a free atom. The ratio e_σ/e_π was fixed to 1/6.[23] Spin orbit interaction was neglected.

The energy position of maxima of the bands for Cr^{4+} and Cr^{3+} centers derived from the absorption and the excitation spectra are summarized in Tables III and V for $Cr:LiScGeO_4$ and $Cr:LiInGeO_4$, respectively.

1. Cr^{4+} *tetrahedral centers*

Figure 6(a) shows crystal axes (a,b,c) and atom positions for the tetrahedral centers, atom positions are listed in Table II (Θ denotes Euler angle relative to the *c*- axis and ϕ is an Euler angle relative to the *a*-axis). Symmetry of local environment is C_s. The energy level diagram for subsequent symmetry reduction T_d-C_{3V}-C_s is shown in Fig. 6(b). The diagram is similar to the diagram for tetrahedral centers in forsterite (Mg_2SiO_4) and cunyite (Ca_2GeO_4) crystals.

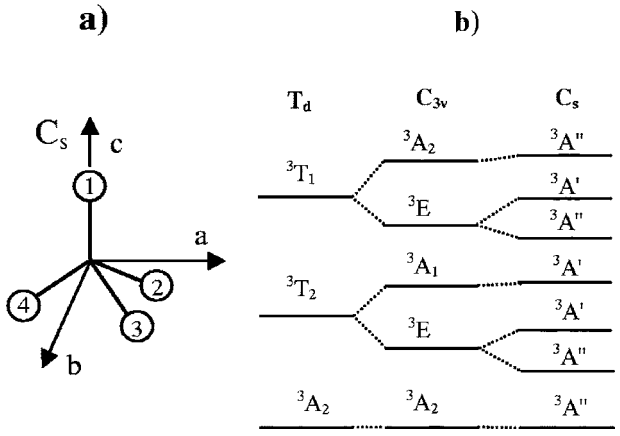

FIG. 6. (a) Orientation of tetrahedral centers and atom assignments (*a*, *b*, and *c* denote crystal axes in *Pnma* notation). (b) Energy level diagram showing energy levels at T_d-C_{3v}-C_s symmetry of the local environment.

The results of AOM calculations for tetrahedral centers are shown in Table III. The agreement between calculated and experimentally observed transition energies is satisfactory. Similar to other Cr^{4+}-doped olivines[18] the distortion of tetrahedrons adequately describes splitting of energy levels in the low-symmetry field. A crystal field strength $10Dq$ parameter is used for the fields with "pure" cubical symmetry and cannot describe low-symmetry crystal fields; however, this parameter can be used as a "mean value" of the crystal field strength for comparison with other materials. $10Dq$ parameter calculated as $4/9(3e_\sigma - 4e_\pi)$ is 9932 and 9790 cm^{-1} for $LiScGeO_4$ and $LiInGeO_4$, respectively. We assign sharp lines from the absorption spectra at $\sim 20\,000-21\,000$ to $^1T_1Cr^{4+}$ transitions because these lines were not detected in the excitation spectra of Cr^{3+} fluorescence. We could not determine positions of possible $^3T_1$(P) transitions because there are strong bands attributed to Cr^{3+} transitions in this range.

Parameters of AOM obtained from the best fit are close those obtained for Cr^{4+}-doped Mg_2SiO_4 and Ca_2GeO_4. The $^3A_2$-^1E transitions were not observed experimentally, similar to Mg_2SiO_4 the ^1E state is found to be (by AOM calculations) the lowest excited state in $LiScGeO_4$ and $LiInGeO_4$ (see Table III). For $Cr^{4+}:Mg_2SiO_4$ this is in contradiction with the assignment of fluorescence to the vibronic $^3T_2$-$^3A_2$ transitions; in $LiScGeO_4$ and $LiInGeO_4$ we did not detect any Cr^{4+} fluorescence neither broadband nor sharp, so no definite conclusion on the lowest excited state can be done.

2. Cr^{3+} *octahedral centers*

Figure 7(a) shows crystal axes (a,b,c) and the axes of octahedron (x,y,z). Octahedron axes are rotated relative to crystal axes. Therefore polarized excitation and absorption spectra are the result of sum of projections of corresponding octahedron axes to the crystal axes. Figure 7(b) shows rotated octahedron for better understanding of its symmetry. In general, symmetry of the distorted octahedrons can be described as a C_s with the mirror plane in the *XZ* plane [see Fig. 7(b)]. Energy level diagram for symmetry reduction

TABLE II. Euler coordinates of the oxygen atoms for tetrahedral positions for $LiScGeO_4$ and $LiInGeO_4$.

	$LiScGeO_4$		$LiInGeO_4$	
Atom	Θ	ϕ	Θ	ϕ
1	2.5	0	2.73	0
2	114.8	180	115.31	180
3	116.8	56.1	117.8	57.16
4	116.8	−56.1	117.8	−57.16

chain O_h-D_{2h}-C_s is shown in Fig. 7(c). Euler coordinates of oxygen atoms are listed in Table IV [Θ denotes Euler angle relative to the z- axis and ϕ is a Euler angle relative to the x-axis, see Fig. 7(b)].

The results of AOM calculation of the transition energies for octahedral centers are summarized in Table V. Experimentally observed maximums of bands derived from the absorption and excitation spectra are also shown in this table. The calculated transition energies are in a reasonable agreement with experimentally observed values taking into account assumptions made to the model and uncertainties in determination of the energies of the bands. In the model we assumed for simplicity that metal-ligand distances are equal for all ligands (in fact they vary within a 7% range); another factor of imperfection can be modification of the local surrounding where a Sc or Li ion is replaced by a smaller Cr^{3+} ion.

In the case of Cr^{3+} centers, transitions cannot be assigned to the certain low-symmetry components of $^4T_2$ splitting because absorption or excitation bands at any polarization are a composition of a few projections of the octahedral axes to the crystal axis. Low-symmetry splitting of the $^4T_2$ state leads to the location of the lowest component at $\sim$12 500–12 800 cm^{-1} (confirmed by both calculations and experiment). Such low energy of the metastable state is the reason for unusual Cr^{3+} octahedral centers near-infrared fluorescence observed in these crystals. Slightly less strength of the crystal field and larger lattice parameters in $LiInGeO_4$

TABLE III. Comparison of absorption band maxima at 20 K and calculated AOM energies of the transitions of the tetrahedral Cr^{4+} centers in $Cr:LiScGeO_4$ and $Cr:LiInGeO_4$ crystals. The AOM parameters are e_σ=9578 cm^{-1}, e_π=1596 cm^{-1}, B=526 cm^{-1} for $LiScGeO_4$ and B=557 cm^{-1}, e_σ=9440 cm^{-1}, e_π=1573 cm^{-1} for $LiInGeO_4$. For both crystals C=4.1B (the free ion ratio).

Transition		$LiScGeO_4$		$LiInGeO_4$	
High spin	Low spin	Calculated (cm^{-1})	Expt. (cm^{-1})	Calculated (cm^{-1})	Expt. (cm^{-1})
	$^1A''(^1E)$	8183		8643	
	$^1A'(^1E)$	8196		8648	
$^3A''(^3T_2)$		9125	8500 (0-0 8250)	8885	8230 (0-0 7930)
$^3A'(^3T_2)$		9192	9400	8958	8840
$^3A'(^3T_2)$		10271	10400	10184	10300
$^3A''(^3T_1)$		13000	12700	12954	12750
	$^1A'(^1A_1)$	13794		14320	
$^3A'(^3T_1)$		13842	14900	13773	14860
$^3A''(^3T_1)$		17338	16900	17582	17210
	$^1A''(^1T_2)$	17240		17455	
	$^1A'(^1T_2)$	17363		17584	
	$^1A'(^1T_2)$	18434		18929	
	$^1A''(^1T_1)$	20046		20703	20480
	$^1A'(^1T_1)$	20532	20310	20952	
	$^1A''(^1T_1)$	21290	21250	21667	
$^3A'(^3T_1(P))$		21622		21495	
$^3A''(^3T_1(P))$		23102		23223	
$^3A''(^3T_1(P))$		23637		23780	

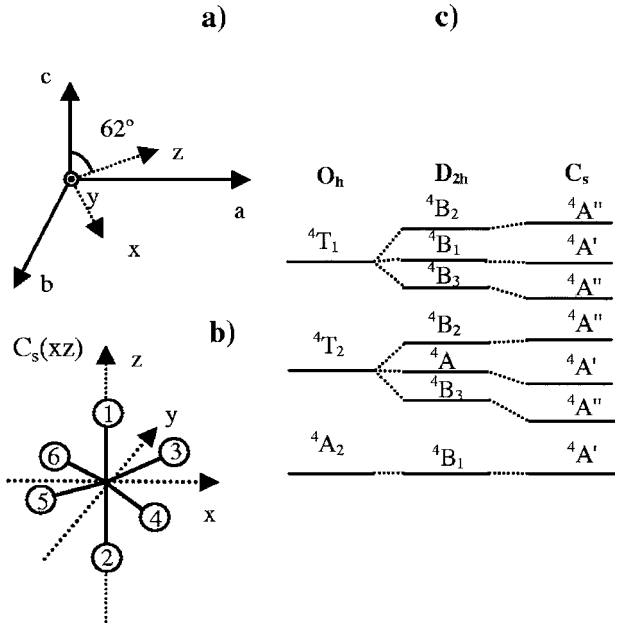

FIG. 7. (a) Orientation of octahedral centers relative to the crystal axes (a, b, and c denote crystal axes in *Pnma* notation and x,y,z denote axes of octahedron); (b) coordinate axes of octahedral center and atom assignment; and (c) energy level diagram showing energy levels at O_h-D_{2h}-C_s symmetry of the local environment.

agree well with the ~300 cm^{-1} low-energy shift of the fluorescence maximum in Cr:$LiInGeO_4$(8730 cm^{-1}) compared to Cr:$LiScGeO_4$(9020 cm^{-1}).

B. Decay of fluorescence

The decay of the fluorescence in both Cr:$LiScGeO_4$ and Cr:$LiInGeO_4$ is a single exponential in the measured range of temperatures (20–360 K) and is independent on wavelength in the whole range of the fluorescence. Temperature dependencies of decay lifetimes are shown in Figs. 8 and 9 by closed circles for $LiScGeO_4$ and $LiInGeO_4$ crystals, respectively. For convenience, the same figures show also the decay rates (calculated as $1/\tau$) by solid triangles. At low temperature the lifetimes of the metastable level are τ=21 and 23 μs, at room temperature they are τ=10.3 and 10.8 μs for $LiScGeO_4$ and $LiInGeO_4$ crystals, respectively.

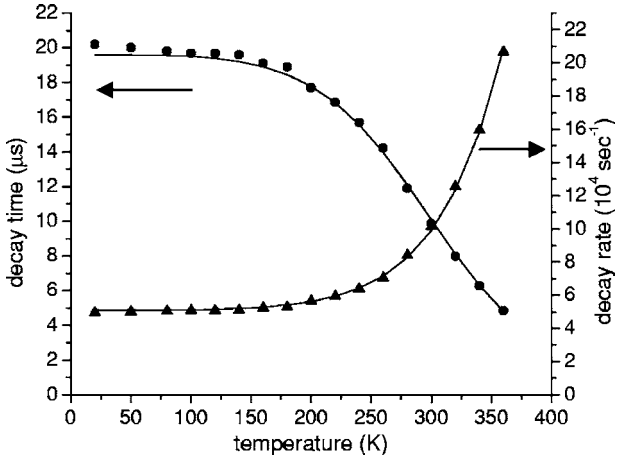

FIG. 8. Temperature dependence of the decay time of the metastable level in Cr:$LiScGeO_4$ (left scale). For convenience the decay rate calculated as $1/\tau$ is also shown (right scale). Experimental data are shown by closed circles and closed triangles, for the decay time and the decay rate, respectively. The best fit by the Struck and Fonger model is shown by a solid curve.

The total decay rate W_{total} of the metastable level is a sum of the radiative decay rate W_r and the nonradiative decay rate W_{nr}:

$$W_{total} = W_r + W_{nr}. \tag{1}$$

A hint about the influence of the radiative rate can be determined by the ratio K of the normalized lifetime τ and normalized integral intensity I of the emission:[24]

$$K = \frac{\tau_{rad}(T)}{\tau_{rad}(T=0)} = \frac{\tau(T)/\tau(T=0)}{I(T)/I(T=0)}. \tag{2}$$

Variations of the K ratio from K=1 are within ~10% for both $LiScGeO_4$ and $LiInGeO_4$ crystals, so we conclude that the rate of the radiative decay changes not significantly with temperature. The temperature dependence of the radiative decay rate on temperature can be neglected in the temperature dependence of the total decay rate and therefore the total decay rate of the metastable level can be described as

TABLE IV. Euler coordinates of the oxygen atoms in the octahedral sites for $LiScGeO_4$ and $LiInGeO_4$.

	$LiScGeO_4$		$LiInGeO_4$	
Atom	Θ	ϕ	Θ	ϕ
1	0	0	0	0
2	179	0	177.5	0
3	89.6	53.8	89.9	53.6
4	89.6	−53.8	89.9	−53.6
5	97.0	−142.8	96.2	−143.5
6	97.0	142.8	96.2	143.5

$$W_{total}(T) = W_{nr}(T) + W_r, \tag{3}$$

where W_r is a constant. From our experimental data we obtain $W_r = 49\,500\ s^{-1}$ for $LiScGeO_4$ and $W_r = 43\,000\ s^{-1}$ for $LiInGeO_4$. The strong temperature dependence of the probability of the decay of the metastable level W is determined mainly by increasing the nonradiative relaxation with temperature.

The temperature quenching of Cr^{3+} fluorescence was not observed for Cr^{3+} centers in forsterite.[25] The reason of temperature quenching of Cr^{3+} fluorescence in $LiScGeO_4$ and $LiInGeO_4$ is a small energy gap between the ground and the metastable level since the probability of nonradiative decay is strongly enhanced with the lower number of phonons bridging the gap. Strong temperature quenching was observed in distorted Cr^{3+} centers in Sc_2O_3 with a small energy gap between the emitting and the ground state levels.[5,6]

The temperature dependence of the nonradiative decay rate can be expressed according to the model of Struck and Fonger:[26,27]

$$W_{nr}(T) = K_{nr}\frac{e^{p-S}}{\sqrt{2\pi p}}\left(\frac{S}{p}\right)^p\left(\frac{p}{p^*}\right)^{1/2}\left(\frac{2p\langle 1+m\rangle}{p+p^*}\right)^p e^{(p^*-p-2mS)}, \tag{4}$$

where $p^* = \sqrt{p^2 + 4S^2\langle 1+m\rangle\langle m\rangle}$, and $\langle m\rangle = 1/(e^{\omega/kT}-1)$, K_{nr} is the nonradiative decay constant, $p = E/\omega$ is the number of phonons bridging the energy gap between the excited state and the ground state (E is the energy of zero-phonon transition), ω is the energy of the effective symmetric even-parity phonon, and S is the Huang-Rhys parameter.

The Huang-Rhys S parameter and phonon energy can be obtained from the spectroscopic data. From the emission spectra (Fig. 3) we see that active centers in $LiScGeO_4$ and $LiInGeO_4$ are characterized by strong electron-phonon coupling with a high value of S and Gaussian bandshape emission curve even at low temperature. At these conditions and $kT \ll \omega$ distribution of the emission intensity $G(E)$ at low temperature is Gaussian:

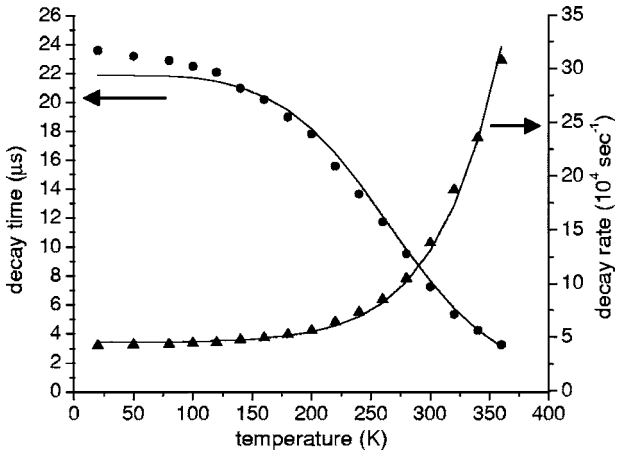

FIG. 9. Temperature dependence of the decay time of the metastable level in Cr:$LiInGeO_4$ (left scale). For convenience the decay rate calculated as $1/\tau$ is also shown (right scale). Experimental data are shown by closed circles and closed triangles, for the decay time and the decay rate, respectively. The best fit by the Struck and Fonger model is shown by the solid curve.

$$G(E) \sim e^{-[E-(E_0+S\omega)]^2/2S(\sigma)^2}, \tag{5}$$

where E_0 is the enegy of zero-phonon transition. We did not detect any zero-phonon lines, but since absorption and emission bands are symmetrical relative to zero-phonon transition E_0 can be estimated as $E_0 = (E_{abs} + E_{fluor})/2$, where E_{abs} is the lowest absorption band maximum and E_{flour} is the maximum of the emission band. The E_0, S, and ω obtained from the best fit are listed in the upper part of Table VI.

TABLE V. Experimental band maxima and calculated AOM energies of the transitions of the octahedral Cr^{3+} centers in Cr:$LiScGeO_4$ and Cr:$LiInGeO_4$ crystals. The AOM parameters are $B = 738\ cm^{-1}$, $e_\sigma = 6670\ cm^{-1}$, $e_\pi = 1110\ cm^{-1}$ for $LiScGeO_4$ and $B = 746\ cm^{-1}$, $e_\sigma = 6530\ cm^{-1}$, $e_\pi = 1088\ cm^{-1}$ for $LiInGeO_4$. For both crystals $C = 4.2B$ (the free ion ratio).

Transition		$LiScGeO_4$		$LiInGeO_4$	
High spin	Low spin	Calculated (cm^{-1})	Expt. (cm^{-1})	Calculated (cm^{-1})	Expt. (cm^{-1})
$^4A''(^4T_2)$		12830	13420	12450	12800
	$^2A''(^2E)$	14515		14660	
	$^2A'(^2E)$	14560	14540	14700	14680
$^4A'(^4T_2)$		14900	13900	14622	13650
$^4A''(^4T_2)$		14980	14500	14700	14000
	$^2A'(^2T_1)$	15090		15210	
	$^2A''(^2T_1)$	15110		15270	
	$^2A'(^2T_1)$	15300	15280	15400	15370
$^4A''(^4T_1)$		21000	21200	20780	20600
$^4A'(^4T_1)$		21020	20800	20800	20700
$^4A''(^4T_1)$		21400	20800	20850	20700

TABLE VI. The energy of zero-phonon line E_0, Huang-Rhys S parameter, and the energy of effective phonon ω derived from the spectroscopic data; and the nonradiative decay constant K_{nr}, S, ω parameters obtained from the best fit by the Struck and Fonger model.

Parameter	$LiScGeO_4$	$LiInGeO_4$
From absorption and emission spectra		
$E_0(cm^{-1})$	11010	10640
S	8.2	7.2
$\omega(cm^{-1})$	250	280
From the best fit of temperature dependencies of lifetime using Struck and Fonger model		
$K_{nr}(s^{-1})$	10^{13}	10^{13}
S	8.0	8.3
$\omega(cm^{-1})$	347	344

These parameters were used as starting parameters to fit temperature dependence of the decay rates (with subtracted value for W_r). The best fit is shown in Figs. 8 and 9 by a solid line and parameters of the best fit are listed at the bottom part in Table VI. As we can see from curves in Figs. 8 and 9, the Struck and Fonger model describes well the experimentally observed values in the whole range of temperatures (20–360 K). The parameters of the best fit are in a satisfactory agreement with those measured independently from the spectroscopic data taking into account simplifications done to the model.

The quantum efficiency of Cr^{3+} emission at room temperature is determined by $\eta(300)=W_r/W_{total}(300)$ and equal to ~50% and ~32% in $LiScGeO_4$ and $LiInGeO_4$, respectively.

V. SUMMARY

The spectroscopic properties of trivalent and tetravalent chromium centers in $Cr:LiScGeO_4$ and $Cr:LiInGeO_4$ have been studied by low temperature absorption, emission, and excitation spectroscopies. Two types of optical centers were found: Cr^{3+} ions in octahedral positions and Cr^{4+} ions in tetrahedral positions. Experimentally observed energies of electronic transitions satisfactory agree with those calculated from exact atom positions using the angular overlap model for both types of optical centers. The decay of the fluorescence obey the Struck and Fonger model, the parameters of the model were derived from the best fit to experimental data. The results reported in this paper confirm our preliminary conclusion on the Cr^{3+} origin of the active fluorescence centers responsible for the ultrabroadband Cr^{3+} near-infrared emission and laser operation recently discovered by us in these crystals.

ACKNOWLEDGMENT

This study was supported by a NASA-URC grant.

[1] J. C. Walling, H. P. Jenssen, R. C. Morris, E. W. O Dell, and O. G. Petersen, Opt. Lett. **4**, 182 (1979).
[2] A. A. Kaminskii, A. P. Shkadarevich, B. V. Mill, V. G. Koptev, and A. A. Demidovich, Inorg. Mater. **23**, 618 (1987).
[3] V. Petricevic, S. K. Gayen, R. R. Alfano, K. Yamagishi, H. Anzai, and Y. Yamaguchi, Appl. Phys. Lett. **52**, 1040 (1988).
[4] N. B. Angert, N. I. Borodin, V. M. Garmash, V. A. Zhitnyuk, A. G. Okhrimchuk, O. G. Siyuchenko, and A. V. Shestakov, Sov. J. Quantum Electron. **18**, 73 (1988).
[5] S. Kück, L. Fornasiero, E. Mix, and G. Huber, J. Lumin. **87–89**, 1122 (2000).
[6] S. Kück, Appl. Phys. B: Lasers Opt. **72**, 515 (2001).
[7] M. Sharonov, V. Petricevic, A. Bykov, and R. Alfano, Opt. Lett. **30**, 851 (2005).
[8] V. Petricevic, A. B. Bykov, J. M. Evans, A. Seas, A. Delgado, R. R. Alfano, and G. V. Kanunnikov, CLEO **CTuE7**, 77 (1997).
[9] A. B. Bykov, G. V. Kanunnikov, and A. L. Bratys, Inorg. Mater. **29**, 278 (1993).
[10] A. Bykov, V. Petricevic, M. Sharonov, J. Steiner, L. Isaacs, T. Avrahami, R. DiBlasi, S. Sengupta, and R. R. Alfano, J. Cryst. Growth **274**, 149 (2005).
[11] M. Yu. Sharonov, A. B. Bykov, V. Petricevic, and R. R. Alfano, Opt. Commun. **231**, 273 (2004).
[12] Heribert Adamsky, *AOMX, An Angular Overlap Model Computer Program*, Theoretical Chemistry (Heinrich-Heine-Universitaet Duesseldorf, 1995).
[13] V. Petricevic, A. Bykov, J. M. Evans, and R. R. Alfano, Opt. Lett. **21**, 1750 (1996).
[14] E. Genkina, V. Timofeeva, and A. Bykov, Zh. Strukt. Khim. **27**, 167 (1986) (in Russian).
[15] M. Touboul and P. Toledano, Acta Crystallogr., Sect. C: Cryst. Struct. Commun. **C43**, 2004 (1987).
[16] W. Jia, H. Liu, S. Jaffe, and W. M. Yen, Phys. Rev. B **43**, 5234 (1991).
[17] A. A. Galeev, N. M. Khasanova, C. Rudowicz, G. S. Shakurov, A. B. Bykov, G. R. Bulka, N. Nizamutdinov, and V. M. Vi-

nokurov, J. Phys.: Condens. Matter **12**, 4465 (2000).
[18] M. F. Hazenkamp, H. U. Güdel, M. Atanasov, U. Kesper, and D. Reinen, Phys. Rev. B **53**, 2367 (1996).
[19] A. Lempicki, L. Andrews, S. J. Nettel, B. C. McCollum, and E. I. Solomon, Phys. Rev. Lett. **44**, 1234 (1980).
[20] M. Voda, J. Garcia Sole, F. Jaque, I. Vergara, A. Kaminskii, B. Mill, and A. Butashin, Phys. Rev. B **49**, 3755 (1994).
[21] U. Fano, Phys. Rev. **124**, 1866 (1961).
[22] M. D. Sturge, H. J. Guggenheim, and M. H. L. Pryce, Phys. Rev. B **2**, 2459 (1970).
[23] D. Reinen, U. Kesper, M. Atanasov, and J. Roos, Inorg. Chem. **34**, 184 (1995).
[24] M. Yamaga, Y. Gao, F. Rasheed, K. P. O'Donnell, B. Henderson, and B. Cockayne, Appl. Phys. B: Photophys. Laser Chem. **51**, 329 (1990).
[25] V. Petricevic, S. K. Gayen, and R. R. Alfano, Appl. Opt. **28**, 1609 (1989).
[26] C. W. Struck and W. H. Fonger, J. Lumin. **10**, 1 (1975).
[27] W. H. Fonger and C. W. Struck, J. Chem. Phys. **69**, 4171 (1978).